Apparent Anomalous Temperature Dependence of Self-Diffusion Studied by Pulsed-Field Gradient Nuclear Magnetic Resonance and Thermodynamic Modeling

Sujeet Dutta, Andrei Nossov, Anne Galarneau, Youcef Didi, Bilel Said, Renaud Denoyel,, Véronique Wernert, Benoit Coasne, Flavien Guenneau

Apparent Anomalous Temperature Dependence of Self-diffusion Studied by Pulsed-Field Gradient Nuclear Magnetic Resonance and Thermodynamic Modeling

Sujeet Dutta,[*,†] Andrei Nossov,[†] Anne Galarneau,[‡] Youcef Didi,[‡] Bilel Said,[‡] Renaud Denoyel,[¶] Veronique Wernert,[¶] Benoit Coasne,[*,§,‖] and Flavien Guenneau[*,†]

† *Sorbonne Université, CNRS, Laboratoire de Chimie de la Matière Condensée de Paris, LCMCP, 75252 Paris, France*

‡ *Institut Charles Gerhardt Montpellier, Univ Montpellier, CNRS, ENSCM, 34293 Montpellier, France*

¶*Aix-Marseille Université, CNRS, MADIREL, UMR 7246, Centre Saint-Jérôme, F-13397, Marseille Cedex 20, France*

§ *Univ. Grenoble Alpes, CNRS, LIPhy, F-38000 Grenoble, France*

‖ *Institut Laue-Langevin, F-38042 Grenoble, France*

E-mail: sujeetpolymer08@gmail.com; benoit.coasne@univ-grenoble-alpes.fr; flavien.guenneau@sorbonne-universite.fr

Abstract

The self-diffusivity of cyclohexane and n-octane adsorbed in hierarchical zeolite monoliths has been investigated using PFG-NMR. In these samples, the intrinsic FAU-X zeolite microporosity combines with a complex macroporous network composed of aggregated zeolite nanocrystals. As temperature is increased, cyclohexane self-diffusivity apparently decreases, reaches a minimum, and then starts increasing upon further rising the temperature. Such striking, i.e. non-Arrhenius, temperature dependence is not observed for n-octane in the same samples and for cyclohexane adsorbed in purely microporous FAU-X. Through thermodynamic modeling, we show that this anomalous behavior can be rationalized by considering the evolution in the adsorbate populations when changing the temperature. In more detail, we show that the slow and fast diffusing species present in the microporosity and secondary porosity arising from the packing of zeolite nanocrystals vary significantly with a strong impact on the effective diffusivity. Applying the temperature evolution of their relative fractions to a simple two-phase diffusion model helps obtain insights into the physico-chemical factors responsible for the complex behavior of effective self-diffusivity in hierarchical zeolites.

TOC Graphic

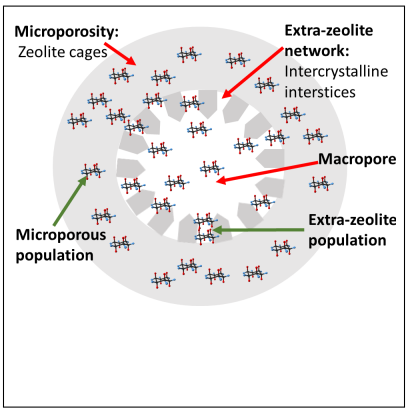

Increasing efforts are put towards maximizing the microporous volume utilization of industrial zeolites with the aim of improving their efficiency in catalysis, gas separation, and purification.[1–3] The ongoing trend is to combine the zeolite microporosity to a network of larger interconnected pores ($\sim$ 10 nm to µm). By designing zeolites with such hierarchical porosity, faster molecular diffusion and, hence, enhanced access to the microporosity can be achieved.[4–10] However, the transport resistance encountered while traveling across different porosity domains can adversely affect the overall self-diffusivity.[11–14] Such hurdles necessitate design optimization of the porous architecture through a thorough understanding of the self-diffusion characteristics of a given adsorbate within an interconnected porous network.

In this context, pulsed field gradient nuclear magnetic resonance (PFG NMR) has proven effective in determining molecular self-diffusion in porous media in the millisecond time scale and micrometer length scale.[15] In more detail, this technique allows one to use different time and spatial resolutions in order to probe self-diffusivity within a single domain or across multiple domains.[7,16] Such information can be interpreted by appropriate physical models to rationalize the multiscale diffusive transport occurring in hierarchical zeolites, as reported previously for n-alkanes and cyclohexane as probe molecules.[4,6,7] This technique has been effective in broadly distinguishing the self-diffusivity of the adsorbed molecules in different porous domains (micro/mesoporosity), therefore giving insights on the network topology.[12,17] However, it is essential to note that the signal attenuation in PFG NMR experiments comprises all the nuclear spins of the adsorbed phase and, hence, gives an effective self-diffusion coefficient of the system. The motivation of this study lies in applying PFG NMR to understand the impact of hierarchical porous architecture on the molecular self-diffusion occurring in multimodal porous zeolites. Equally important is to understand the dependence of such information on the choice of the probe molecule adsorbed within these porous networks. The enthalpy of adsorption of the guest molecule, its vapor pressure, competition between the guest–guest and guest–host molecular interactions, and the diffusion mechanism of the adsorbate are important physical parameters affecting the diffusion dynamics and eventual

information that can be gathered about the porous network topology. In this regard, we elaborate in this manuscript, the critical role played by the thermodynamic and molecular interactions between the chosen probe molecule and the porous host in obtaining a correct assessment of the PFG NMR data.[8,12,17]

We focus here on a series of hierarchical Faujasite-X (FAU-X) monoliths that combine the zeolite cages (microporosity) with an interconnected network of macropores (1 µm–20 µm). In more detail, the skeletons in these hierarchical monoliths are composed of FAU-X micro-/nanocrystals depending on the sample, as shown in Fig. 1 (a) and Fig. S1 (a) and (b) (supporting information). Such materials have been reported to exhibit outstanding ability to trap Cs^+ îons in water with ideal breakthrough curves revealing high mass transfer and no external diffusion limitations.[18,19] A thorough understanding of the topology of these zeolites is essential to rationalize and further optimize such performance. In this regard, the molecular self-diffusion of cyclohexane and *n*-octane adsorbed in the hierarchical FAU-X monoliths was investigated over a broad temperature range.

Cyclohexane and *n*-octane were adsorbed in four different FAU-X monoliths: (i) Fau_0; purely microporous commercial FAU-X microystals powder compressed into a monolith, (ii) Fau_{m1}; hierarchical FAU-X composed of FAU-X microcrystals and possessing small macropores ($\sim 1\,\mu m$), (iii) Fau_{m2}; hierarchical FAU-X composed of FAU-X nanocrystals and possessing large macropores ($\sim 17\,\mu m$), and (iv) Fau_{m3}; hierarchical FAU-X composed of FAU-X nanocrystals and possessing small macropores ($\sim 1\,\mu m$). All the monoliths were of cylindrical geometry with a 5 mm diameter and a length ranging between 10–15 mm. The hierarchical FAU-X monoliths were produced by the pseudomorphic transformation of hierarchical macroporous/mesoporous silica monoliths prepared by a combination of sol-gel method and spinodal decomposition.[19] Details of the synthesis procedure are provided in the Supporting Information. X-ray diffraction patterns of the hierarchical monoliths confirm the crystallographic structure of FAU-X [see Fig. S1(c), (d), and (e) in the Supporting Information].

Fig. 1(a) compares the microstructure of the three synthesized FAU-X monoliths with

the purely microporous sample, Fau_0. The zeolite crystal sizes are listed in Table S1 of the Supporting Information. The largest zeolite particles in Fau_{m1} (microcrystals) are approximately 2 µm in size and are comparable to the Fau_0 crystals. On the other hand, Fau_{m2} and Fau_{m3} clearly feature smaller crystals ($\sim$ 300 nm). Fig. S2(e) in the Supporting Information shows the N_2 sorption isotherms for the three synthesized FAU-X monoliths and the compressed Fau_0 sample. The corresponding microporous volumes, V_μ, are listed in Table S1 of the Supporting Information. The extra-zeolite network (macroporosity and secondary porosity arising from inter-crystalline interstices) was characterized using Hg porosimetry. Table S1 also lists the macroporous volumes, V_m, and macropore diameters, d_m, of the various FAU-X monoliths. We observe that the compression of the Fau_0 powder into a monolith gives rise to some excess free volume (0.44 mL/g) due to imperfect compaction, which may be considered equivalent to a macroporous network. Fau_0 and Fau_{m1} exhibit comparable macroporous diameters ($\sim$ 1 µm). Fig. S2(a) in the Supporting Information reveals that the secondary porosity increases in the order: $Fau_0 < Fau_{m1} < Fau_{m2} < Fau_{m3}$. This order is reflected in the specific surface areas of the monoliths [see Table S1 and Fig. S2 (b) in the Supporting Information]. Evidently, the hierarchical FAU-X zeolites offer a complex secondary region for adsorption spanning multiple length scales of confinement, the impact of which on the overall self-diffusion dynamics of the probe molecules is presented in this study.

Cyclohexane and *n*-octane were chosen as probe molecules for the topological investigation of the FAU-X samples. Fig. 1(b) shows the cyclohexane (full circles)/ *n*-octane (open squares) adsorption isotherms in the FAU-X samples (experimental details can be found in the Supporting Information). Typically, in zeolites, complete filling of the microporosity is indicated by a saturation in the adsorbate loading (*y*-axis, mmol/g). In the case of Fau_0, both for cyclohexane and *n*-octane, the filling saturation occurs at low partial pressures ($P/P_0 \leq 0.4$). However, in the hierarchical FAU-X samples, pore-filling increases continuously with partial pressure due to progressive adsorption in the extra-zeolite framework.

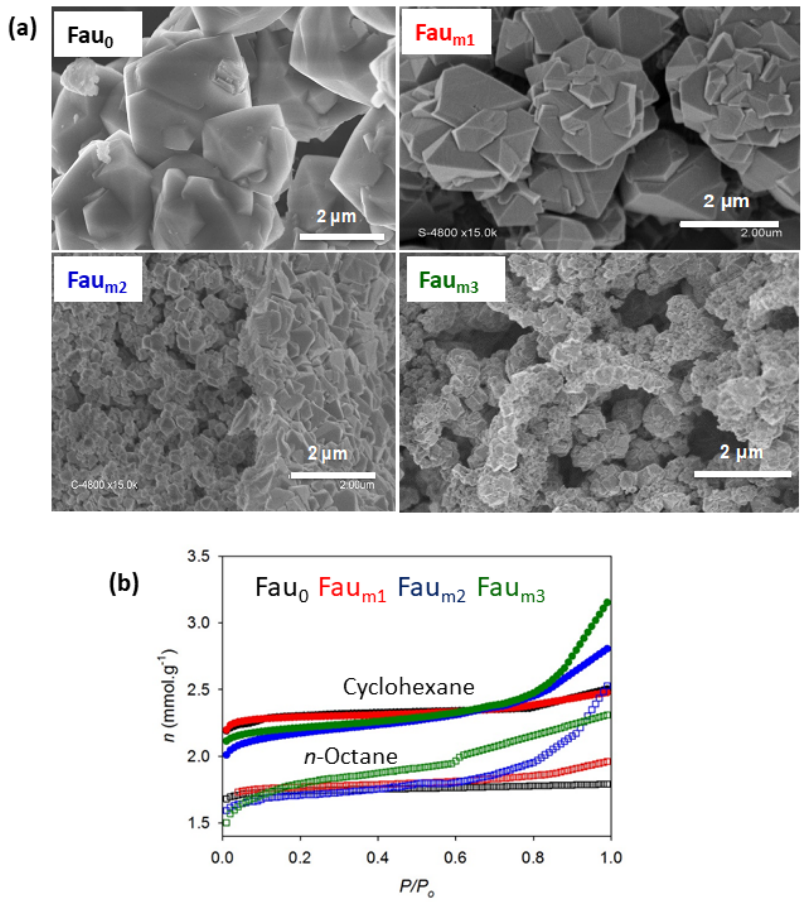

Figure 1: **(a)** SEM images of the four FAU-X samples investigated in this study. **(b)** Cyclohexane and n-octane adsorption isotherms at 298 K for the different samples. Solid circles: cyclohexane, Open squares: n-octane.

This effect is more pronounced in Fau_{m2} and Fau_{m3} featuring nanocrystals than in Fau_{m1} featuring microcrystals. The latter exhibits a significant overlap with Fau_0 until partial pressures, $P/P_0 > 0.7$, are reached. For Fau_0, the amount of cyclohexane/n-octane adsorbed in the microporosity was determined at the partial pressure of saturation of the isotherm – see Fig. 1(b). The values are listed in Table 1 along with the corresponding P/P_0 values. For Fau_{m1},Fau_{m2} and Fau_{m3}, adsorbed amount at microporous filling was estimated by extrapolating the adsorption isotherm [$P/P_0 \sim 0.2$–0.6, see Fig. 1(b)] to $P/P_0 \sim 0$. The values thus determined and the partial pressures to which they correspond are listed in Table 1.

PFG NMR spatially encodes the nuclear spins of a given system by utilizing a pair of spatially dependent magnetic field pulses (the pulse duration is $\approx 1\,\text{ms}$).[20] The strength of

Table 1: Adsorbed amount at complete microporous filling (n_μ) for a given FAU-X–adsorbate pair; actual adsorbed quantity during sample preparation (n_{ads}); quantity adsorbed in excess of microporous capacity (Δn). P/P_0–n_μ and P/P_0–n_{ads} are the partial pressures on the corresponding adsorption isotherms. Refer to Fig. 1(b) for the adsorbate-specific isotherms. Fig. 4(a) illustrates the locations of n_{ads}, n_μ, and n_m on cyclohexane adsorption isotherm curves in Fau_{m1} as an example.

		Cyclohexane			
FAU-X	n_μ (mmol/g)	P/P_0–n_μ	n_{ads} (mmol/g)	Δn (mmol/g)	P/P_0–n_{ads}
Fau_0	2.3	0.19	2.3	0	0.19
Fau_{m1}	2.27	0.19	2.3	0.03	0.27
Fau_{m2}	2.26	0.48	2.5	0.24	0.84
		n-Octane			
Fau_0	1.73	0.15	1.76	0.03	0.54
Fau_{m1}	1.75	0.1	1.76	0.01	0.13
Fau_{m2}	1.65	0.06	1.76	0.09	0.42
Fau_{m3}	1.73	0.12	1.76	0.03	0.15

the gradient pulses and time resolution between them can be varied to set the observation length and time scale of the molecular displacements under investigation.[15,16,21] Further details of its basic principles are provided in the Supporting Information. The NMR signal (net magnetization) attenuation, Ψ ($= I/I_0$), can be expressed as:

$$\Psi(g\gamma\delta, \Delta) = \exp -[(g\gamma\delta)^2 D_s \Delta], \tag{1}$$

where g and δ are the strength and duration of the gradient pulse, respectively. γ is the gyromagnetic ratio of the nucleus being studied (here, ^{1}H) and Δ is the observation time. Thus, the self-diffusion coefficient, D_s, of any molecular species can be determined from the slope of the attenuation $\ln \Psi$ versus $(g\gamma\delta)^2\Delta$ plot (with small adjustments depending on the pulse sequence actually used).[21,22]

Typically, the self diffusivity of molecules in bulk or when confined only in a single porous domain is represented by a single linear slope.[23] However, in hierarchical porosities, the confined molecules may traverse through multiple domains depending upon the Δ value used.[24] If Δ is smaller than the time required to cross from one domain to another, the signal

attenuation will exhibit a multi-exponential curve. In that case, D_s within each domain can still be determined from $\ln \Psi$ versus $(g\gamma\delta)^2\Delta$ plot. However, for sufficiently large Δ, a molecule traverses through multiple domains so that each domain affects the inferred self diffusivity.[7] As a result, in that case, $\ln \Psi$ represents the effective diffusivity, D_{eff}, of all molecules probed simultaneously traversing across all domains. The quantity $g\gamma\delta$ (with units of m^{-1}) is analogous to the scattering vector in diffraction experiments and is referred to as q in this manuscript. In PFG NMR experiments, for fixed δ and Δ values, the strength of the gradient pulse g primarily determines the length scale being probed.[21,22]

Each FAU-X monolith was evacuated under vacuum at $\sim 300\,^{\circ}C$ inside an NMR tube to remove any pre-adsorbed molecules. Thereafter, it was immersed in liquid N_2 and its pores were filled by condensing cyclohexane/n-octane from the vapor phase. Then, after reaching equilibrium, the NMR tube was flame sealed. The pressure at which the adsorbate was filled in the FAU-X monoliths corresponded to 100% filling of the microporous volume, V_{micro}, obtained from the N_2-sorption isotherms [see Table S1 and Fig. S2(d) of the Supporting Information]. In doing so, it was assumed that the adsorbate is at its bulk liquid density within the microporosity. The amount of cyclohexane/n-octane filled in each FAU-X monolith is listed in Table 1. As seen in Table 1, this sample preparation procedure leads to slight excess filling for nearly all the monoliths when compared with the microporous capacity deduced from cyclohexane/n-octane adsorption isotherms (this amount is noticeably higher for Fau_{m2}). We note that, due to the chemical potential equality between the fluid adsorbed in the microporosity, in the extra-zeolite network, and in the gas phase, the presence of fluid adsorbed at the meso-/macropore surface cannot be avoided. In our previous work, we demonstrated via thermodynamic modelling that such excess adsorbed quantities tend to dynamically evolve with temperature. Since the NMR signal attenuation in such cases comprises the net effective diffusivity of more than one dynamic population, each being sensitive to changes in temperature, we risk misinterpreting the NMR data if a clear understanding of such evolution is not present.[4] The eventual miscalculation of the associated diffusion

coefficients may lead to erroneous understanding of the topological effects of complex porous media.

The PFG NMR experiments were initially carried out at 25 °C to investigate the effect of Δ on the attenuation. Technical details of the PFG NMR measurements, such as the strength of the magnetic field, pulse sequence used, and the associated experimental parameters can be found in the Supporting Information. As an example, Fig. 2(a) shows the signal attenuation for cyclohexane and *n*-octane adsorbed in Fau_{m1}. Here, the x-axis is expressed in $q^2\Delta$ with $q = g\gamma\delta$. According to Eq. (1), the slope of $\ln \Psi$ versus $q^2\Delta$ yields the effective self-diffusion coefficient D_{eff}, the variation of which with Δ is plotted in Fig. 2. We find that D_{eff} decreases slightly with increasing Δ values, indicating that the adsorbed molecules traverse across mulitple porous domains without encountering significant surface resistance from the zeolite network. Fig. S2(a) and (b) of the Supporting Information show signal attenuation of cyclohexane adsorbed in Fau_0 and Fau_{m2} at different Δ values, respectively. The corresponding D_{eff} values are plotted against Δ in Fig. S2(d) of the Supporting Information. Please note that the system cyclohexane/Fau_{m3} could not be included in this study owing to the fast self-diffusion dynamics of cyclohexane in this monolith, causing rapid signal attenuation and low SNR even for the shortest Δ (0.5 ms) applicable in our NMR setup. Table S2 lists the Δ values selected for each cyclohexane/FAU-X system for conducting systematic PFG NMR experiments between 278–328 K. This value was chosen to maximize the SNR, therefore optimizing the accuracy of the inferred diffusion coefficients. On the other hand, the use of different – albeit comparable – Δ prevents the direct comparison of the different samples. This aspect is left for further study as the present work is mostly devoted to understanding how the thermodynamics of adsorption impacts self-diffusion measurements in such complex systems. Fig. S2(c) of the Supporting Information shows the signal attenuation for *n*-octane adsorbed in Fau_{m2} and Fau_{m3} at different Δ. A wide range of Δ values could not be explored for the *n*-octane based systems owing to strong reduction in SNR with increasing Δ, thereby making it difficult to assess the impact of surface barriers

on self-diffusion. The Δ value thus chosen for systematic PFG NMR experiments between 278–328 K for each *n*-octane/FAU-X system was based on the highest SNR achieved at 25 °C (Table S2 in the Supporting Information).

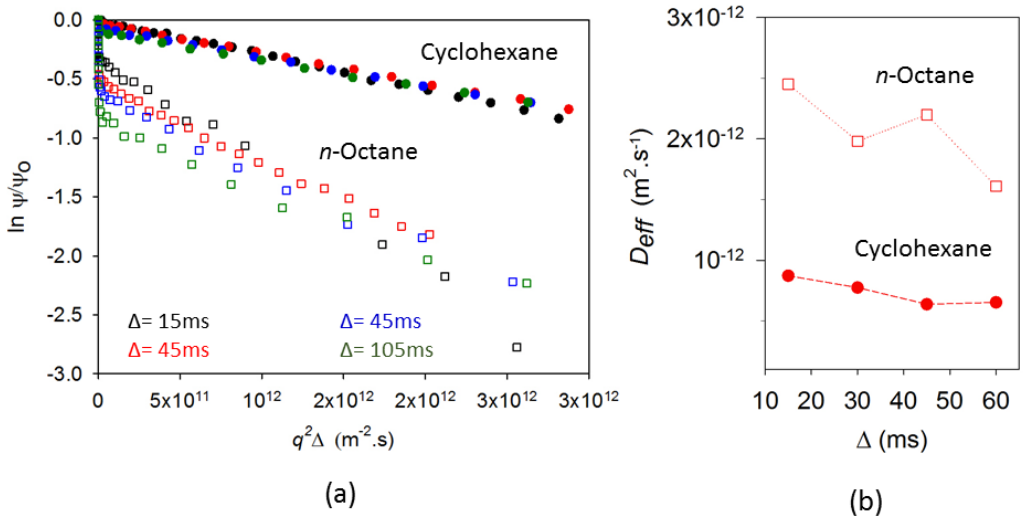

Figure 2: **(a)** NMR signal attenuation, $ln\Psi$, plotted against $q^2\Delta$ ($q = g\gamma\delta$) at 298 K for cyclohexane (solid circles) and *n*-octane (open squares) adsorbed in Fau_{m1}. The data are shown for different Δ values as indicated in the legend. **(b)** Dependence of D_{eff} on Δ for cyclohexane (solid circles) and *n*-octane (open squares) adsorbed in Fau$_m$1.

Fig. S3 of the Supporting Information shows the attenuation curves for different FAU-X/adsorbate systems at a few selected temperatures to illustrate the influence of temperature on molecular self-diffusion. For cyclohexane/Fau$_{m1}$, *n*-octane/Fau$_0$, *n*-octane/Fau$_{m2}$, and *n*-octane/Fau$_{m3}$ [Fig. S3(a), (b), (f), and (g) of the Supporting Information, respectively]. ln Ψ exhibits only a single slope, therefore indicating that the self-diffusion in the entire monolith is described by a single D_{eff}. In contrast, for cyclohexane/Fau$_{m1}$ and *n*-octane/Fau$_{m1}$ [Fig. S3(c) and (d) of the Supporting Information], ln Ψ rapidly decreases at low magnetic field gradient strength (corresponding to $q < 5 \times 10^{10}\,\mathrm{m^{-2}\,s}$). This may be attributed to fast

molecular exchange between the adsorbed and vapor phases. This comprises a small fraction of the overall signal attenuation and is disregarded for the estimation of D_{eff} as the focus of this study is on the self-diffusion of molecules in the adsorbed phase. For cyclohexane/Fau_{m2} [Fig. S3(e) of the Supporting Information], we observe – especially at 288 K and 298 K – that $\ln \Psi$ gradually decreases until $q \sim 3 \times 10^{10}\,\text{m}^{-2}\,\text{s}$. This corresponds again to molecules that diffuse, at least partially, in the gas phase. Beyond this regime, a single slope is present as we increase the gradient strength, which can be attributed primarily to molecular diffusion in the micropores. As a result, D_{eff} for cyclohexane/Fau_{m2} were extracted from the attenuation curves beyond $q \sim (2.5 \pm 0.5) \times 10^{10}\,\text{m}^{-2}\,\text{s}$.

D_{eff} obtained at different temperatures for each FAU-X/adsorbate pair are plotted versus temperature in Fig. 3. As expected, D_{eff} for *n*-octane increases with temperature – albeit at a different rate in each FAU-X monolith. In contrast, we observe that cyclohexane exhibits a non-intuitive behavior in the hierarchical FAU-X monoliths. Indeed, D_{eff} for Fau_{m1} and Fau_{m2} decrease with increasing temperature until reaching a minimum threshold at 308 K and 313 K, respectively. Upon further increasing the temperature, D_{eff} increases proportionately. Surprisingly, this behavior was not observed for cyclohexane adsorbed in Fau_0 monolith, which is simply a compressed powder and lacks a genuine hierarchical structure. Such anomalous temperature dependence is thermodynamically unfeasible as an increase in thermal energy must translate into greater kinetic energy for the adsorbate molecules and, thus, lead to a strict increase in D_{eff} (as exhibited by *n*-octane for instance). Such a fundamental disagreement in the self-diffusivity of different adsorbates poses a serious difficulty in choosing an appropriate molecule for topological probing. In what follows, we explore the underlying thermodynamic reasons behind such a contrasting behavior between the dynamics of these two probe molecules.

Redistribution between microporosity and extra-zeolite porosity. For cyclohexane adsorbed in Fau_{m1}/Fau_{m2}, we hypothesize a scenario of progressive dominance of a dynam-

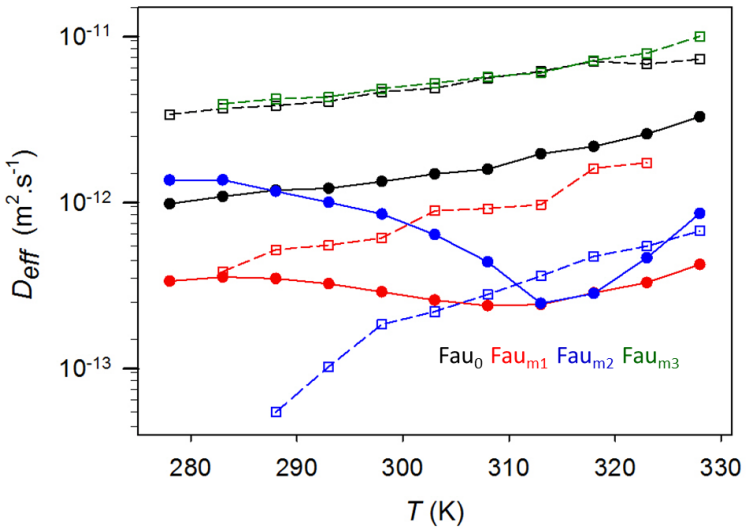

Figure 3: Effective self-diffusion coefficients D_{eff} for cyclohexane (full circles) and n-octane (open squares) adsorbed in different FAU-X samples as a function of temperature.

ically slower molecular population being probed. Concomitantly, a faster moving fraction of molecules is gradually being depleted. In such a scenario, the minima in D_{eff} versus T indicates the temperature at which the slowly diffusing population becomes dominant. An Arrhenius rise of D_{eff} upon increasing the temperature further (> 308 K for Fau$_{m1}$ and > 313 K for Fau$_{m2}$) indicates that the dynamically slower population is the only existing adsorbed molecular species that follows the expected thermodynamic behavior. Typically, there are three different molecular populations that could be envisaged in our adsorbate/FAU-X systems: (1) molecules present in microporosity (zeolite cages), (2) molecules adsorbed in the secondary porosity offered by the extra-zeolite framework, and (3) molecules in the gas phase within the macropores of the monolith. As shown below, we propose that during the exchange of molecules between the microporosity and macroporous gas phase, a small fraction of them adsorb in the extra zeolite framework. In more detail, we explain this population redistribution between the three domains by a thermodynamic model proposed in one of our previous works.[4] To do so, we combine the thermodynamic model of Polanyi and the Frenkel-Halsey-Hill theory to predict the adsorption isotherm of a given adsorbate/FAU-X pair at a target temperature from its experimental adsorption isotherm at a known tem-

perature.[4,25–28] As derived by W. Kellouai et al.,[28] the underlying hypothesis is that the chemical potential of the adsorbed phase $\mu(T, P)$ at a given temperature and pressure (T, P) is equivalent to its value $\mu_0(T, P_0)$ in the liquid phase at the saturating vapor pressure P_0 corrected for the interaction potential, E, between the adsorbate and adsorbent surface. Under this consideration, the adsorbed volume written as the product of the total adsorbed amount, N, and molar volume, v, of the adsorbate (assumed to be equivalent to its bulk liquid value) is assumed to be temperature invariant. While this approximation at the heart of the Polanyi adsorption potential theory can appear as questionable, it can be understood and rationalized as follows. It simply assumes that the adsorbed phase possesses a liquid-like structure that resembles that of the bulk liquid at the same temperature. In particular, the volume occupied by N adsorbed molecules is taken as $N_v(T)$ where $v(T)$ is the bulk molar volume at temperature T. As shown by Kellouai et al., this approximation was found to be robust for both a nanoconfined fluid and an adsorbed fluid at an external surface.[28] This implies that molecules would readily adsorb in all sites of energy, E, as long as the condition $\mu - \mu_0 = E$ is fulfilled. Moreover, assuming the gas phase behaves ideally, the physical quantity $Nv[\mu - \mu_0(T), T]$ can be expressed as a function of P and P_0 at a given temperature: $Nv = f[k_B T\ lnP/P_0(T)]$. Through the above equation, we used the experimental N versus P curves (adsorption isotherms) of the FAU-X/adsorbate pairs at 298 K [Fig. 1(b)] to predict their corresponding adsorption isotherms between 278–328 K. As an example, Fig. 4(a) shows the adsorption isotherms for cyclohexane adsorbed in Fau_{m1}. The red curve is experimentally obtained at 298 K while the black and blue curves are those predicted by the above-mentioned thermodynamic treatment for 288 K and 308 K, respectively.

Note that only the low partial pressure region ($P/P_0 < 0.5$) of the adsorption isotherms is shown to illustrate the estimation of adsorbed quantities in the microporosity and extra-zeolite framework, respectively. The total adsorbed amount per unit mass of a FAU-X monolith (in mmol/g) is given by $n_{ads} = n_\mu + n_m$, where n_μ and n_m denote the specific adsorbed quantities in the microporosity and extra-zeolite porosity, respectively. The total

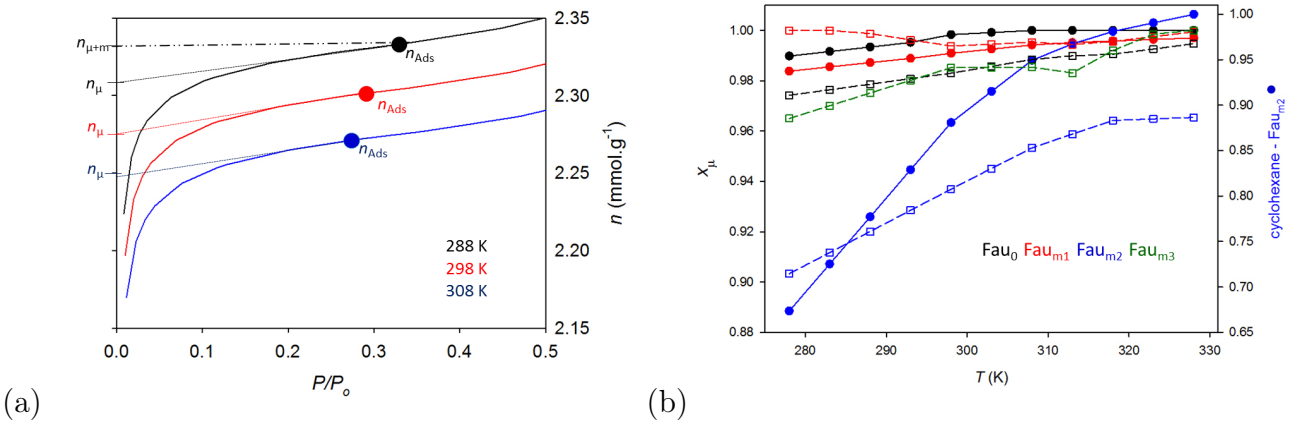

Figure 4: **(a)** Adsorption isotherms at 288 K (black) and 308 K (blue) obtained from the experimental curve at 298 K (red) using our thermodynamic model. The total adsorbed quantity, n (expressed here per unit mass of the monolith; mmol/g), consists of the adsorbate in micropores, n_μ, and the extra-zeolite porosity, n_m, combined. n_μ is obtained by linear extrapolation of the adsorption isotherm to $P/P_0 \sim 0$. n_m is obtained by deducting n_μ from n. **(b)** x_μ, the fraction of adsorbate present in the microporosity (see legend) as obtained from the thermodynamic treatment. Cyclohexane: full circles, n-Octane: open squares. The secondary y-axis-scale on the right represents the cyclohexane/Fau_{m2} system. The solid and dashed lines are guides for the eye.

number of moles of guest molecules in the entire system (monolith inside the sealed NMR tube) can be calculated as follows:

$$N = N_{ads} + N_g = n_{ads} m_0 + \frac{(V_d + V_m)P}{RT}, \tag{2}$$

where N is the total quantity of guest molecules (in mol) present in the NMR tube at sample preparation. N_{ads} is the total adsorbed quantity in the FAU-X monolith. N_g is the quantity of molecules in the gas phase, which is present in the dead volume of the NMR tube, V_d, and the macroporous volume, V_m, of the monolith combined. The dead volume is the section of the NMR tube that excludes the volume occupied by the monolith. In practice, $V_d >>> V_m$, such that $V_d + V_m \approx V_d$. m_0 is the mass of the empty monolith. R is the universal gas constant. P is the vapor pressure of the gas phase determined from the adsorption isotherm of a given adsorbate/FAU-X pair at a specified temperature T (here, we note that the gas is assumed to behave ideally – which is justified considering the low

pressures considered in this work). Since the sample is present in a sealed environment, N is constant at all temperatures. As a result, it can be determined by interpolation from a given adsorption isotherm using Eq. (2) for a temperature T. The corresponding P/P_0 helps determine n_{ads} ($= N_{ads}/m_0$) on the adsorption isotherm as illustrated in Fig. 4(a). Since n_μ is determined beforehand via extrapolation, the quantity adsorbed in the extra-zeolite framework is simply determined using $n_m = n_{ads} - n_\mu$.

The relative fractions of the guest molecules in the microporosity and extra-zeolite porosity are thus given by:

$$\chi_{\mu/m/g-mono} = \frac{N_{\mu/m/g-mono}}{N_{ads} + N_{g-mono}}. \tag{3}$$

Here, $\chi_{\mu/m/g-mono}$ denotes the mole fraction of guest molecules in the microporosity/extra-zeolite porosity/macroporous volume of the FAU-X monolith, respectively. N_μ and N_m are the absolute quantities of adsorbate present in the microporosity and extra-zeolite network, respectively. $N_{g-mono} = V_m P/RT$ is the quantity of molecules in the gas phase within the macroporous volume of the monolith.

Interpreting the self-diffusion coefficients. Having established the redistribution of the adsorbate population between the microporosity and extra-zeolite network, and its evolution with temperature, we investigate their impact on the effective self-diffusivity of the system. The root-mean-square displacements $\langle u^2_{rms}\rangle^{1/2}$ of the adsorbed guest molecules are given by: $\langle u^2_{rms}\rangle \sim 6\Delta D_{eff}$. The range of $\langle u^2_{rms}\rangle^{1/2}$ calculated for the different adsorbate/FAU-X pairs from their corresponding D_{eff} values are listed in Table S2. Comparing these values with the corresponding particle sizes (see Table S1), and considering the Δ used, molecular diffusion seems to be restricted within the microporosity in Fau_0 and Fau_{m1}. While the Arrhenius temperature dependence of D_{eff} for cyclohexane in Fau_0 supports this assumption (Fig. 3), the anomalous behavior in Fau_{m1} indicates a more complex situation.

The molecular diffusion mechanism inside zeolite cages (microporosity) can vary depend-

ing on the molecular structure of the guest molecule. For example, cage-to-cage hopping is expected for aromatic molecules and configurational diffusion for linear chain alkanes. On the other hand, for the extra-zeolite network that is comprised of macropores, the mechanism is essentially Fickian. In our study, since we focus on the micrometer length scale and millisecond timescale, the diffusion mechanism within the microporosity is assumed to be Fickian as well. Owing to its simplicity, we first attempt to explain the observed self-diffusion behavior with the *fast-exchange model*.[6,16] This model assumes a Fickian diffusion regime, wherein the trajectory segments of molecular diffusion in different domains of a multi-domain system are uncorrelated. As a result, the effective diffusion coefficient for a system consisting of m different domains (microporosity, secondary porosity, etc.) can be determined according to the following equation:

$$D_{eff} = lim_{t\to\infty}\ \frac{1}{6t}\sum_{n=1}^{m}\langle(\sum_{\iota}\Delta r_{\iota}^{n})^{2}\rangle, \tag{4}$$

where Δr_{ι}^{n} is the ι^{th} trajectory segment traversed by a molecule in the domain n in time t. Here $\langle(\sum_{\iota}\Delta r_{\iota}^{n})^{2}\rangle$ is the mean square sum of molecular displacements in all the domains combined.[6] The latter quantity can be approximated as $6t_nD_n$, where t_n is the proportion of time spent in domain n and D_n is the corresponding self-diffusion coefficient in that domain. By invoking ergodicity, we assume the proportion of time spent by molecules in a given domain $\tau_n = t_n/t$ is equal to the fraction of molecules present in the domain at a given time. As a result, the effective diffusivity, D_{eff}, can be expressed as:

$$D_{eff} = \sum_{n=1}^{n}\chi_n D_n = \chi_\mu D_\mu + \chi_m D_m + \chi_g D_g \tag{5}$$

where χ_n is the fraction of molecules present in domain n. The second equality corresponds to our system which contains microporosity μ, extra-zeolite porosity m, and gas phase g. During the experiments, the NMR tube is positioned within the magnetic field and radio-frequency coil such that only the monolith is present inside it. Therefore, the gas phase in Eq. 5 comprises the cyclohexane/n-octane molecules that may diffuse in the macroporosity while

exchanging between different regions of the extra-zeolite framework. We estimated $D_g \sim 10^{-7}\ \mathrm{m^2\,s^{-1}}$ for cyclohexane and n-octane using Knudsen diffusion in macropores of diameter 10^{-6} m. This value is much higher than the experimentally obtained self-diffusion coefficients for both cyclohexane and n-octane ($1 \times 10^{-13}\ \mathrm{m^2\,s^{-1}}$ and $1 \times 10^{-11}\ \mathrm{m^2\,s^{-1}}$, respectively). This indicates that the contribution of the gas phase is better represented by the fast attenuation at low field gradients [e.g. Fig. 2(a) and Fig. S3 of the Supporting Information], which we have excluded from our analysis.

Thus, for fitting our experimental data we focus solely on a bi-domain model, wherein the effective diffusivity is written as a weighted linear combination of diffusivity in the microporosity and extra-zeolite network that depends on their relative proportions (x_μ and x_m, respectively). As a result, Eq. (5) simplifies to $D_{eff} = x_\mu D_\mu + x_m D_m$ (with $x_{\mu/m} = n_{\mu/m}/n_{ads}$).

Fig. 4(b) shows the evolution of x_μ with temperature for the different adsorbate/FAU-X pairs. The full circles and open squares represent cyclohexane and n-octane, respectively. Fig. S4(a) and (b) of the Supporting Information show the corresponding plots of n_μ and n_m versus temperature, respectively. These plots illustrate that even if both n_μ and n_m decrease with increasing temperature due to the adsorbed molecules escaping to the gas phase, x_μ tends to increase with temperature and gradually saturate to a maximum value. The only outlier in this set is n-octane/Fau$_{m1}$ as x_μ appears to globally decrease with increasing temperature T. This apparent behavior results from a small rise in n_m (≈ 0.01 mmol/g between 278–328 K), which is quite small with respect to the decrease in n_m observed for other FAU-X/adsorbate pairs [≈ 0.04 mmol/g; Fig. S4(b) of the Supporting Information]. Thus, we consider that n_m does not change significantly for n-octane/Fau$_{m1}$ with temperature. In turn, we assume its apparent rise and fall (fall and rise in x_μ, respectively) to be within the error range of estimates from the thermodynamic treatment (± 0.01 mmol/g).

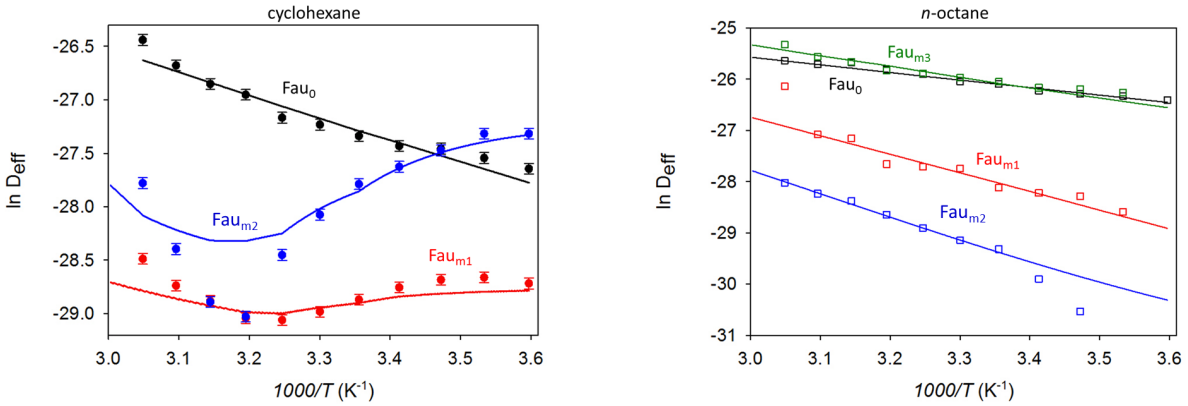

(a) (b)

Figure 5: Fit of the experimental D_{eff} (see figure 3) using our model described in the main text. Solid circles and open squares represent the experimental D_{eff} values for **(a)** cyclohexane and **(b)** n-octane, respectively. The solid lines are the fits of the experimental points, the results of which are listed in Table 2.

The effective self-diffusion coefficient $D_{eff}(T)$ at any temperature T can be expressed as:

$$D_{eff}(T) = x_{\mu}(T)D_{\mu}(T) + [1 - x_{\mu}(T)]D_{m}(T), \tag{6}$$

where $D_{\mu/m}(T)$ at any given temperature are expressed in the Arrhenius form as:

$$D_{\mu/m}(T) = D^{278}_{\mu/m} \ \exp\left[\frac{E_{\mu/m}}{R}\left(\frac{1}{278} - \frac{1}{T}\right)\right].^{4} \tag{7}$$

Here $x_{\mu}(T)$ is the fraction of adsorbate in the microporosity at a given temperature, while the corresponding fraction in the extra-zeolite network can be simply written as $x_m(T) = 1 - x_{\mu}(T)$. $D^{278}_{\mu/m}$ are the reference diffusion coefficients at 278 K, while $E_{\mu/m}$ are the activation energies for diffusion in the microporosity and extra-zeolite regions, respectively. With x_{μ} versus T known from the thermodynamic model [Fig.4 (b)], we fit the experimental data with $D^{278}_{\mu/m}$ and $E_{\mu/m}$ as the fitting parameters. Fig. 5(a) and (b) show D_{eff} in log scale for cyclohexane and n-octane in the different FAU-X monoliths. The symbols represent the experimental points, while the solid lines are fits to the experimental curves using Eq. 6 and 7. The result of the fitting procedure is shown in Table 2.

Table 2: Result of fit from the ln D_{eff} versus $1/T$ curves shown in Fig. 5 for cyclohexane and *n*-octane. The subscripts μ and m denote the microporous and extra-zeolite regions, respectively.

		Cyclohexane		
Fau-X Monolith	D_μ^{278} ($\mathrm{m^2\,s^{-1}}$)	E_μ ($\mathrm{kJ\,mol^{-1}}$)	D_m^{278} ($\mathrm{m^2\,s^{-1}}$)	E_m ($\mathrm{kJ\,mol^{-1}}$)
Fau_0	8.2×10^{-13}	18.1	5×10^{-12}	13
Fau_{m1}	2.4×10^{-14}	33	1.8×10^{-11}	10
Fau_{m2}	2.2×10^{-14}	51	4.1×10^{-12}	13
		Octane		
Fau_0	3.1×10^{-12}	13	1×10^{-11}	10
Fau_m1	2.8×10^{-13}	30	1×10^{-12}	10
Fau_m2	5.5×10^{-14}	38	2×10^{-13}	10
Fau_m3	2.7×10^{-12}	18	9.5×10^{-12}	10

As seen in Fig. 5(a), there is a quantitative mismatch between the theoretical predictions and experimental points for cyclohexane. Yet, a qualitative prediction of the trend of experimental points is achieved. This implies that the values of physical quantities for cyclohexane listed in Table 2 are indicative of a rather complex physical scenario that is over-simplified in the diffusion model used here. Nevertheless, being able to predict the anomalous "V-shaped" trend of D_{eff} versus T for cyclohexane offers us important insights. (1) The self-diffusivity of cyclohexane in the microporous domain of the hierarchical FAU-X samples is much lower (2–3 orders of magnitude) than in the extra-zeolite porosity. In contrast, this is not the case for *n*-octane and for cyclohexane adsorbed in $\mathrm{Fau_0}$. (2) The microporosity of hierarchical FAU-X samples offers considerable transport resistance to molecular diffusion compared to $\mathrm{Fau_0}$, indicated by the lower D_μ^{278K} and higher activation energies (see Table 2) for both cyclohexane and *n*-octane. Further, a direct comparison of E_μ, the activation energy of microporous diffusion, between the different hierarchical zeolites cannot be made. Meanwhile, the activation energy for diffusion in the extra-zeolite region is comparable for the three zeolite monoliths used in this study, which also happens to be comparable to the activation energy of diffusion in bulk cyclohexane.[4] In effect, this implies that the extra-zeolite population has liquid-like features.

Under these considerations, an increasing proportion of microporous adsorbate popula-

tion, x_μ, leads to the following implication. Upon increasing the temperature, the slower species dominates while the faster one (adsorbed in the extra-zeolite network) contributes increasingly lesser to the measured D_{eff}. Given the small values of x_m, the contribution of molecules diffusing in the extra-zeolite network can be practically ignored and the experimentally obtained D_{eff} values would represent microporous diffusion. This is typically the case for n-octane adsorbed in all the FAU-X samples used in this study and for the cyclohexane/Fau$_0$ system. However, if the difference between D_μ and D_m is significant, the impact of extra-zeolite population on the effective diffusion coefficient can be considerable. Thus, a gradual reduction in the extra-zeolite population with increase in temperature would manifest itself as an apparent decrease in effective diffusivity (as observed for cyclohexane adsorbed in the hierarchical FAU-X samples). This scenario can typically be accentuated if the initial extra-zeolite population is higher, such as for the cyclohexane/Fau$_{m2}$ system. Once the extra-zeolite population is below a certain threshold (e.g. for $T > 308$ K for cyclohexane), D_{eff} is strongly dominated by microporous diffusion and the following rise in its values with temperature is nothing but an expected trend of Arrhenius increase in microporous diffusivity.

On the contrary, n-octane diffusion in the zeolite happens to be non-anomalous, and the quality of fits appears reasonably good as a result. The drawback for n-octane, however, is that the exact same observation time could not be used to probe its diffusion in the different zeolite samples, which again makes a direct comparison of diffusion in the different zeolite samples difficult. However, on qualitative grounds, the high activation energy associated with microporous diffusion in the samples Fau$_{m1}$ and Fau$_{m2}$ indicates that a higher transport resistance is encountered by the diffusing molecules in these two samples.

The present study illustrates the importance of the probe molecule selected for topological studies of hierarchical porous media. Though cyclohexane has been a popular choice for such investigations in the past, the anomalous temperature dependence of its self-diffusion dynamics in the monolithic hierarchical FAU-X zeolites used in this study raises serious

concerns. Using our thermodynamic model, we reveal that the adsorbate population redistributes itself into two broad domains; the microporosity (zeolite cages) and the extra-zeolite network/secondary porosity arising from the packing of zeolite crystals. In our systems, the proportion of microporous population is overwhelmingly higher than in the extra-zeolite network. Further, the thermodynamic treatment reveals that the proportion of microporous population of the adsorbate tends to increase with temperature, which naturally leads to an increase in its contribution to the effective self-diffusivity as well. Through a simple two-phase diffusion model, we qualitatively establish that an increase in temperature may lead to an apparent lowering of the effective self-diffusivity if the self-diffusion dynamics in the extra-zeolite network is significantly faster than in the microporosity (as observed for cyclohexane in the present study for instance). Such scenarios might as well occur for other adsorbate/porous matrix systems necessitating a careful choice for appropriate probe molecule(s) for topological investigation of hierarchical porous materials. In future work, molecular simulations could be used to provide fundamental insights into the diffusive behavior of cyclohexane and *n*-octane in microporous/mesoporous zeolites. Few relevant molecular models are already available in the literature based on simple flat interface between a zeolite and a larger pore or a cylindrical mesopore inside a zeolite crystal.[5,28] However, considering the typical time scales ($\sim$ 100 ns) that can be reached with molecular dynamics, the maximum mean squared displacement probed by a molecule with a very low diffusivity ($\sim 10^{-12}\mathrm{m}^2\,\mathrm{s}^{-1}$) will be less than $1\,\mathrm{nm}^2$. Given the typical self-diffusivity observed experimentally for such fluidic populations, such a value is clearly insufficient to reach the Fickian regime and hence probe self-diffusivity with enough confidence.

Supporting Information Statement

Details of the synthesis and characterization of hierarchical FAU-X monoliths. **Fig. S1:** SEM and XRD, **Fig. S2:** Hg porosimetry and N_2 sorption of FAU-X monoliths. Details of

cyclohexane/n-octane adsorption experiments in the hierarchical FAU-X and corresponding data (**Table S1**).**Fig. S3 and S4:**Dependence of NMR signal attenuation on the observation time, Δ, and temperature for the different adsorbate/FAU-X pairs, respectively. The corresponding root-mean-square displacements are listed in **Table S2**.

Acknowledgement

The authors thank the French National Research Agency (Agence Nationale de la Recherche) for their financial support through the ANR TAMTAM 15-CE08-0008 grant.

References

(1) Verboekend, D.; Pérez-Ramírez, J. Design of Hierarchical Zeolite Catalysts by Desilication. *Catal. Sci. Technol.* **2011**, *1*, 879–890.

(2) Mardiana, S.; Azhari, N. J.; Ilmi, T.; Kadja, G. T. Hierarchical Zeolite for Biomass Conversion to Biofuel: A Review. *Fuel* **2022**, *309*, 122119.

(3) Yang, J.; Yuan, N.; Xu, M.; Liu, J.; Li, J.; Deng, S. Enhanced Mass Transfer on Hierarchical Porous Pure Silica Zeolite Used for Gas Separation. *Microporous Mesoporous Mater.* **2018**, *266*, 56–63.

(4) Dutta, S.; Galarneau, A.; Minoux, D.; Aquino, C.; Dath, J.; Guenneau, F.; Coasne, B. Molecular Diffusion in Hierarchical Zeolites with Ordered Mesoporosity: Pulsed Field Gradient Nuclear Magnetic Resonance Combined with Thermodynamic Modeling. *J. Phys. Chem. C* **2023**, *127*, 1548–1559.

(5) Coasne, B.; Galarneau, A.; Gerardin, C.; Fajula, F.; Villemot, F. Molecular Simulation of Adsorption and Transport in Hierarchical Porous Materials. *Langmuir* **2013**, *29*, 7864–7875.

(6) Galarneau, A.; Guenneau, F.; Gedeon, A.; Mereib, D.; Rodriguez, J.; Fajula, F.; Coasne, B. Probing Interconnectivity in Hierarchical Microporous/Mesoporous Materials Using Adsorption and Nuclear Magnetic Resonance Diffusion. *J. Phys. Chem. C* **2016**, *120*, 1562–1569.

(7) Galarneau, A.; Mehlhorn, D.; Guenneau, F.; Coasne, B.; Villemot, F.; Minoux, D.; Aquino, C.; Dath, J.-P. Specific Surface Area Determination for Microporous/Mesoporous Materials: The Case of Mesoporous FAU-Y Zeolites. *Langmuir* **2018**, *34*, 14134–14142.

(8) Mehlhorn, D.; Valiullin, R.; Kärger, J.; Schumann, K.; Brandt, A.; Unger, B. Transport Enhancement in Binderless Zeolite X-and A-type Molecular Sieves Revealed by PFG NMR Diffusometry. *Microporous Mesoporous Mater.* **2014**, *188*, 126–132.

(9) Mehlhorn, D.; Rodriguez, J.; Cacciaguerra, T.; Andrei, R.-D.; Cammarano, C.; Guenneau, F.; Gedeon, A.; Coasne, B.; Thommes, M.; Minoux, D. et al. Revelation on the Complex Nature of Mesoporous Hierarchical FAU-Y Zeolites. *Langmuir* **2018**, *34*, 11414–11423.

(10) Schneider, D.; Mehlhorn, D.; Zeigermann, P.; Kärger, J.; Valiullin, R. Transport Properties of Hierarchical Micro–Mesoporous Materials. *Chem. Soc. Rev.* **2016**, *45*, 3439–3467.

(11) Gueudré, L.; Jolimaître, E.; Bats, N.; Dong, W. Diffusion in Zeolites: Is Surface Resistance a Critical Parameter? *Adsorption* **2010**, *16*, 17–27.

(12) Kaerger, J. In-depth Study of Surface Resistances in Nanoporous Materials by Microscopic Diffusion Measurement. *Microporous Mesoporous Mater.* **2014**, *189*, 126–135.

(13) Sastre, G.; Kärger, J.; Ruthven, D. M. Diffusion Path Reversibility Confirms Symmetry of Surface Barriers. *J. Phys. Chem. C* **2019**, *123*, 19596–19601.

(14) Sastre, G.; Kärger, J.; Ruthven, D. M. Surface Barriers and Symmetry of Adsorption and Desorption Processes. *Adsorption* **2021**, *27*, 777–785.

(15) Kärger, J.; Pfeifer, H. NMR Self-Diffusion Studies in Zeolite Science and Technology. *Zeolites* **1987**, *7*, 90–107.

(16) Kärger, J.; Pfeifer, H.; Heink, W. *Advances in Magnetic and Optical Resonance*; Elsevier, 1988; Vol. *12*; pp 1–89.

(17) Kärger, J.; Valiullin, R. Mass Transfer in Mesoporous Materials: The Benefit of Microscopic Diffusion Measurement. *Chem. Soc. Rev.* **2013**, *42*, 4172–4197.

(18) Didi, Y.; Said, B.; Micolle, M.; Cacciaguerra, T.; Cot, D.; Geneste, A.; Fajula, F.; Galarneau, A. Nanocrystals FAU-X Monoliths as Highly Efficient Microreactors for Cesium Capture in Continuous Flow. *Microporous Mesoporous Mater.* **2019**, *285*, 185–194.

(19) Didi, Y.; Said, B.; Cacciaguerra, T.; Nguyen, K. L.; Wernert, V.; Denoyel, R.; Cot, D.; Sebai, W.; Belleville, M.-P.; Sanchez-Marcano, J. et al. Synthesis of Binderless FAU-X (13X) Monoliths with Hierarchical Porosity. *Microporous Mesoporous Mater.* **2019**, *281*, 57–65.

(20) Stejskal, E. O.; Tanner, J. E. Spin Diffusion Measurements: Spin Echoes in the Presence of a Time-Dependent Field Gradient. *J. Chem. Phys.* **1965**, *42*, 288–292.

(21) Price, W. S. Pulsed-Field Gradient Nuclear Magnetic Resonance As a Tool for Studying Translational Diffusion: Part 1. Basic Theory. *Concepts in Magnetic Resonance: An Educational Journal* **1997**, *9*, 299–336.

(22) Price, W. S. Pulsed-Field Gradient Nuclear Magnetic Resonance As a Tool for Studying Translational Diffusion: Part II. Experimental Aspects. *Concepts in Magnetic Resonance: An Educational Journal* **1998**, *10*, 197–237.

(23) Kukla, V.; Kornatowski, J.; Demuth, D.; Girnus, I.; Pfeifer, H.; Rees, L. V.; Schunk, S.; Unger, K. K.; Kärger, J. NMR Studies of Single-File Diffusion in Unidimensional Channel Zeolites. *Science* **1996**, *272*, 702–704.

(24) Sørland, G. H. *Dynamic Pulsed-Field-Gradient NMR*; Springer, 2014; pp 37–61.

(25) Rouquerol, J.; Rouquerol, F.; Llewellyn, P.; Maurin, G.; Sing, K. S. *Adsorption by Powders and Porous Solids: Principles, Methodology and Applications*; Academic press, 2013.

(26) Neimark, A. V.; Grenev, I. Adsorption-induced Deformation of Microporous Solids: A New Insight From a Century-old Theory. *J. Phys. Chem. C* **2019**, *124*, 749–755.

(27) Coasne, B.; Gubbins, K. E.; Pellenq, R. J.-M. Temperature Effect on Adsorption/Desorption Isotherms For a Simple Fluid Confined Within Various Nanopores. *Adsorption* **2005**, *11*, 289–294.

(28) Kellouai, W.; Judeinstein, P.; Plazanet, M.; Baudoin, S.; Drobek, M.; Julbe, A.; Coasne, B. Gas Adsorption in Zeolite and Thin Zeolite Layers: Molecular Simulation, Experiment, and Adsorption Potential Theory. *Langmuir* **2022**, *38*, 5428–5438.